Industry Paper

Proposed Small Observation Rover with Six In-wheel Motors for Precision Agriculture

Kenji Terada*
Masaki Endo*, Takuo Kikuchi*, Shigeyoshi Ohno*
* Division of Core, Polytechnic University, Japan
{k-terada, endou, kikuchi, ohno}@uitec.ac.jp

Abstract - Japanese agriculture is confronting the simultaneous difficulties of an aging population, diminishing numbers of workers, and increased area of arable land. Therefore, smart agriculture using IoT and robots is attracting attention. As a crop condition observation technology, UAVs have been attracting attention. Nevertheless, observing pests and diseases under leaves is impossible, although that is the main avenue of crop damage. Therefore, we propose a small agricultural rover that can provide above-ground images of leaf undersides and environmental information that can support important decision-making for precision agriculture. This paper describes the structure of a small agricultural rover that can provide stable observations for sustainable crop production in an orchard.

Keywords: agriculture, IoT, robot, sensing

1 INTRODUCTION

Undoubtedly, agriculture is an important economic sector worldwide. However, the Japanese agricultural sector particularly is confronting the difficulties of an aging population and a severe labor shortage. As numbers of agricultural enterprises continue to shrink in Japan, the average amount of arable land per farmer is expected to expand [1]. Therefore, great interest has arisen in smart agriculture systems. Farmers must increasingly use the internet of things (IoT) and robot technology to acquire and analyze highly accurate data related to diverse crop production factors to realize precision agriculture [2]. These demands have hastened the development of useful farm machinery [3 - 4].

Particularly, AI-based systems are finding new value in agricultural management. Currently, a cloud service that uses sensors to measure environmental conditions to predict harvest and disease outbreaks is in practical use [5]. For example, services worldwide assess disease damage from images of plants taken by farmers with smartphones and other devices [6 - 9]. An inexpensive system that uses crop images to monitor crop growth is expected to increase agricultural efficiency. It is also expected to reduce the risk of crop failure in areas where there are few skilled farmers. In another study, remote sensing technology using an unmanned aerial vehicle (UAV) is used to monitor growing conditions through images. With the advent of UAVs, it has become easier to collect data to support farm growth management [10]. However, estimating growing conditions from aerial images taken by UAVs requires ground-truth: actual measurements. Moreover, aerial photography by UAVs is not a panacea. Ground observations are necessary (Fig. 1).

Figure 1: Diseases and pests on the leaf underside.

Figure 2: Virus carrier on the leaf underside on farms owned by co-developers.

For example, disease detection from imaging requires visual evaluation such as observation of a single leaf on the ground for early detection of diseases such as powdery mildew on the underside of leaves [11]. These observations are limited to those made from the air. Various crop-damaging pests are parasites that feed on the underside of leaves: lepidopteran pests, coleopterans, spider mites, and snails [12]. If even one virus-diseased plant is missed, an infection might spread to other crops on the same farm, leading to secondary damage. Virus carriers are insects, mollusks, or fungi that parasitize leaf underside (Fig. 2).

The Ministry of Agriculture, Forestry, and Fisheries of Japan report that efforts to prevent the spread of plant diseases and pests can contribute to SDGs 1, 2, 8, 12, 13, 15, and 17 [13]. The amount of damage caused by such diseases is said to exceed 100 billion yen per year [14].

Herein, we propose a small agricultural rover able to observe environmental data and the undersides of crop leaves from the ground to observe crops and manage field variation, which is important for precision agriculture.

The capabilities necessary to make observations using a small rover are the following.

- Driving on uneven terrain with branches and irregular soil composition, topology, and texture
- Collection of environmental parameters such as leaf underside images, temperature, and humidity. while driving between rows of crops
- Use of field maps using data from observations

Observation by a mobile rover is an effective means to achieve low-cost ground observation of the leaf underside for each crop. Observing leaf undersides requires a rover

that can suppress rover swaying caused by various small bumps inherent to farms, such as branches and tread marks. Therefore, the small agricultural rover developed for this study of an orchard has a mechanism with a damper function in the frame body to which the wheels are attached.

For the reasons described above, this study proposes a small agricultural robot that observes the soil and which also takes upward-looking images of crops on a farm to complement agricultural management data obtained from drones and farmers. Section 2 presents explanations of related studies and the position of this study among the relevant literature. Section 3 presents a description of a prototype developed for this research. Section 4 gives the results of prototype driving tests. Section 5 presents the conclusion.

2 RELATED WORK

For this study, the name of the small robot to be developed is the Field Scouting Rover (FSR). Robots of many types patrol farms [15 - 18]. Actually, FSR aims at achieving stable autonomous running on uneven terrain, despite its small size, for close observation of many crops.

As ideas we propose, we consider that an important issue for agricultural robots is the decline in maintenance performance caused by miniaturization. Especially, the aging of the workforce requires not only the easy operation of robots but also easy maintenance of machines. Also, uneven terrain is a necessary part of farm driving. Replacing dampers and other parts used in many agricultural rovers to cope with uneven terrain is a highly specialized task. Therefore, we specifically evaluated a mechanism with a damper function in the frame itself, where the wheels are mounted, to improve ground contact on mildly uneven terrain without increasing the number of parts. This mechanism mitigates the vehicle body's vertical movement and angle changes by connecting all wheels with links (Fig. 3).

Furthermore, to distribute the load, the number of wheels was increased from four to six, which is the number of wheels used in many agricultural robots. Thereby the running performance was improved and tire marks on the farm were reduced. Moreover, the number of parts was reduced by omitting the steering mechanism. This feature particularly addresses a farm's need to travel in straight lines rather than making sharp turns.

The rocker-bogie mechanism used in the Mars explorer is famous as a similar idea. The rocker-bogie mechanism structure can apply an equal load to each wheel, which enables stable operation, even on uneven terrain. However, because of that rocker bogie mechanism structure, a vast difference exists in running performance between the front and rear. Additionally, it has been pointed out that the number of parts increases along with the need for lower height: it is not a simple mechanism [19]. Therefore, the FSR frame has a six-wheeled vehicle mechanism that differs from the rocker bogie mechanism. The rolling mechanism allows the FSR to maintain contact between the ground and the six wheels even when the ground is uneven on both sides. The other mechanism used for reference uses in-wheel motors that are driven separately. Steering is done by differential movement of the left and right wheels [20]. The FSR uses no damper or other complicated parts for the linkage mechanism.

Figure 4 presents the FSR position in farm observations. Observations made by small robots will enable farmers to make better-informed farm management decisions using precision information that is obtainable remotely. If a good farmer observes disease or insect damage in one place, then the farmer will then inspect several places and make a comprehensive judgment.

The FSR is aimed at complementing data obtained by UAVs that make observations from the sky. Thereby, the FSR can observe areas that are difficult for farmers to see, but which farmers must observe, such as crop bases and leaf undersides. FSR is also expected to be used to observe crops near the farm using thermometers, hygrometers, and barometers. Therefore, the FSR will be equipped with a camera for real-time crop observation. The situation can be checked with a smartphone or other device by streaming and storing crop images. The sky will occupy most of the background when the rover looks up at the crop leaves. The amount of background information unrelated to the plant can be reduced. The problem with plant disease diagnosis is that operational performance cannot be ensured for images taken in a different environment because of overtraining that includes background information, which occupies a larger area than that of the plant [21]. By reducing the number of useless background images, the analysis time can be reduced.

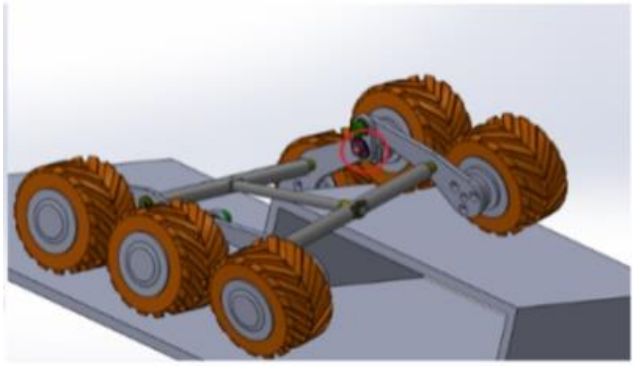

Figure 3: Frame design.

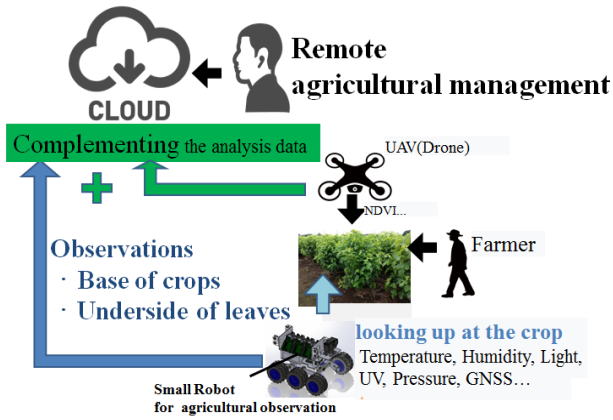

Figure 4: Positioning of FSR for agricultural observations.

3 ROVER DEVELOPMENT

3.1 Specifications of FSR

Table 1 present the FSR specifications. Fruit trees, especially those that use leaves such as mulberry and tea, are harvested once a year. These crops must be observed daily to maintain quality. Spacing between fruit trees in a small orchard is 1,000 mm [22]. From the top, the FSR is the size of an A4 size paper with six wheels. The FSR size is intended to be sufficiently large to observe these crops. Increasing the road-following ability makes it possible to drive stably without the tires floating. An effective way to increase the road-following ability is to make the wheels heavier. The FSR has an in-wheel motor with a built-in motor mechanism. The motor weight increases the wheel weight. The in-wheel motor used for the FSR was selected from commercially available products that can be procured easily. We selected the in-wheel motor for the FSR from commercially available products that were procured easily. The two main points were that the motor should support only one side of the wheel (cantilever) and that it should have sufficient torque to tow its weight to realize the mechanism used in the FSR. We selected parts from a battery-powered E-Skateboard. The frame size was designed based on the selected in-wheel motor diameter. It was sufficiently large to observe an orchard farm.

3.2 Frame of the Body

A frame with an in-wheel motor was designed using " SolidWorks Corporation," as depicted in Fig. 5, after the design, the software simulator was used to check the grounding characteristics. Parts of the frame were fabricated using numerical control machining and a laser machine.

3.3 In-wheel Motor Control

Figure 6 shows the in-wheel motor control circuit. The driver circuit that came with the in-wheel motor could not connect to other electronic circuits. Therefore, we built a circuit using a brushless DC motor driver (TB6605FTG). The in-wheel motors on the market varied in terms of weight and the number of coil turns. In addition, individual speed control is necessary to achieve straight line operation [20]. A microcontroller for in-wheel motor control was provided for each in-wheel motor. The FSR's control microprocessor uses a Jetson Nano. The control circuit is connected to a 2D-LiDAR [RPLIDAR A2M8; Shanghai Slamtec Co. Ltd.]. The 2D-LiDAR enables the detection of obstacles among the surroundings of the FSR. The control microcontroller was constructed to send rotation commands to the microcontroller, which controls each in-wheel motor. To enable BLE communication with smartphone applications, as described in Section 3.5, the microcontroller for control is connected to the BLE module [BLE Serial3]. In addition, the control microcontroller is connected to the gyro sensor [CMPS12], which is located at the center of the FSR's chassis for angle control of turning and other operations. For communication between microcontrollers, microcontrollers use I2C communication. One battery was used for each of the two in-wheel motors to enable testing of the individual motor controls and to facilitate testing of flexible layout adjustments in the FSR. In addition, one battery was used for each of the seven microcontrollers. A Li-Fe battery material was selected: it is lighter and safer than Li-Po. Compared to Li-Po batteries, Li-Fe batteries are formed from materials that are extremely resistant to ignition, making them effective for robots with high vibration. The speed of the FSR for observation was set to 3.2 km/h, which is regarded as a slow human gait [23]. Because the selected in-wheel motor was not designed for low speed, the control microcomputer program had to reduce its responsiveness. Therefore, the program to lower the clock of the timer interrupt used for feedback control in the control microcomputer program made it possible to reduce the motor speed.

Table 1: Specifications of FSR

FSR Length [mm]	350.0
FSR Width [mm]	294.0
FSR Height [mm]	310.0
FSR Weight [kg]	7.4
Wheel diameter [mm]	65.0
Wheel weight [g]	760
Maximum power [kW]	$0.5^{*2} \times 6^{*1}$
Maximum velocity [km/h]	30.3^{*2}
Minimum velocity [km/h]	2.4^{*2}
Average uptime [min]	63.3^{*3}

*1 Number of motors
*2 motor catalog data (over-engineering)
*3 no load

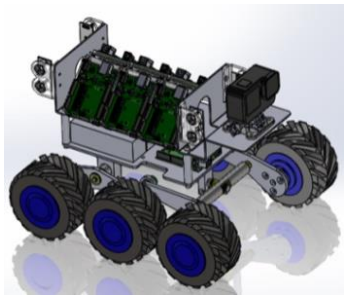

Figure 5: Design and simulation of FSR.

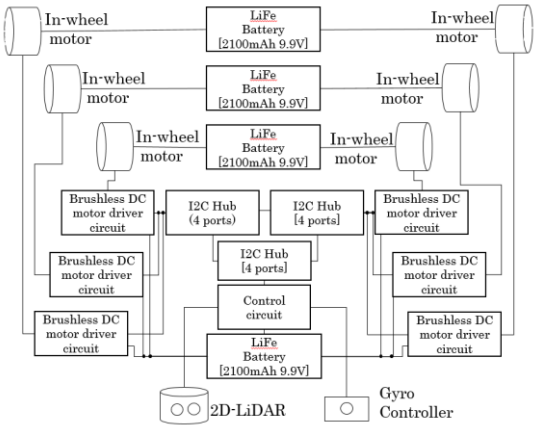

Figure 6: In-wheel motor control system of FSR.

3.4 Log of Environment Sensor Recording Functions

Figure 7 presents a log of FSR environment sensor recording functions used to detect environmental data such as temperature and humidity while taking leaf underside images when driving between rows of crops. Cloud services can collect and store such data. Therefore, sensor connection points must have microcontrollers that can connect to the internet easily. Therefore, the FSR's sensing microprocessor uses a Raspberry pi4 B+. To obtain environmental information on date and time, temperature (°C), humidity (%), light (lx), U-V index, pressure (hPa), and noise (dB), the FSR uses an environmental sensor (2jcie-bl01; Omron Corp.). The sensor can connect the FSR's sensing microprocessor via BLE communication. Thereby, the sensing microprocessor location on FSR can be changed flexibly. To obtain crop images, the sensing processor is connected to a Raspberry Pi HQ Camera. In addition to obtaining the observation location coordinates, the sensing microprocessor is connected to a GPS Module (Ultimate GPS Breakout - 66 channel w/ 10 Hz updates – Version 3; Adafruit Inds.). The program used for observations was produced using Python. The measured environmental information is saved in a CSV file in the sensing microprocessor. Additionally, it uses IoT Core, S3, DynamoDB, OpenSearch Service, etc., which are services of Amazon Web Services, Inc. (AWS), to upload a group of sensor values to a cloud service. The use of cloud services makes remote data observation possible. The sensing microprocessor is installed with a mjpeg-streamer to capture images and distribute images during observation for viewing on a web browser such as a smartphone. Using mjpeg-streamer, one can distribute video and acquire still images using the HTTP protocol. By observing log data gathered by FSR with the program, one can obtain environmental sensor data for crops.

3.5 Smartphone Application to Operate FSR

Figure 8 depicts a screenshot of the smartphone application to operate the FSR. An Android OS smartphone application controls the FSR. The camera image of the sensing microprocessor is projected at the top of the smartphone application screen: a web browser screen. After the user taps the connect button to start communication with the FSR and communication starts, the user can command the FSR to operate by pressing the respective arrow buttons. The FSR stops when the arrow button is released. To experiment with turning the prototype, pressing the automatic button will make the FSR turn when going straight, up to the length (m) entered.

4 EXPERIMENT

It is necessary to verify whether our proposed simple frame with a small number of parts is useful to observe farms.

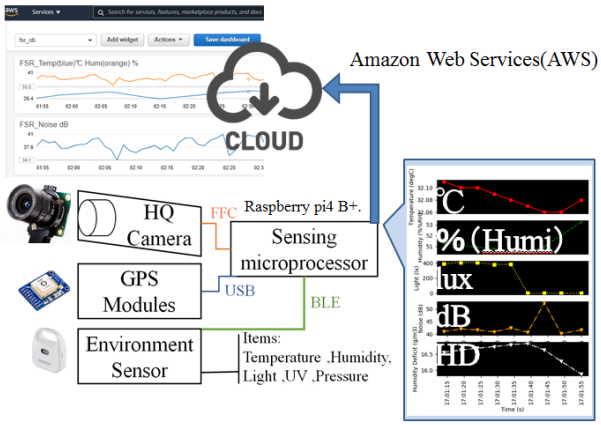

Figure 7: Log of environment sensor recording function of FSR.

Figure 8: Smartphone application to operate FSR.

As described in the *Introduction*, we conducted “Mobility” and “Driving on uneven terrain” experiments to assess driving on uneven terrain with branches and irregular topology. Moreover, a "leaf underside observation" experiment elucidated capabilities for detecting temperature, humidity, and other environmental parameters, along with leaf underside images while driving between rows of crops. Moreover, a field map was produced using observation data.

4.1 Mobility

The FSR is not equipped with a mechanism, such as a constant velocity joint, to change the wheel angle. Figure 9 portrays the FSR movement on a farm. First, to realize stable observation on a farm, FSR needs straight-line control. It also needs control to change the turning radius according to the size of the crop being grown on the farm. Turning is achieved by speed differences between the left and right wheels. Therefore, we analyzed those characteristics during turning by controlling the in-wheel motor speed.

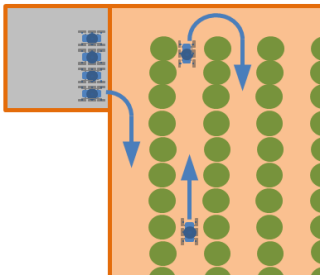

Figure 9: FSR in action on a farm.

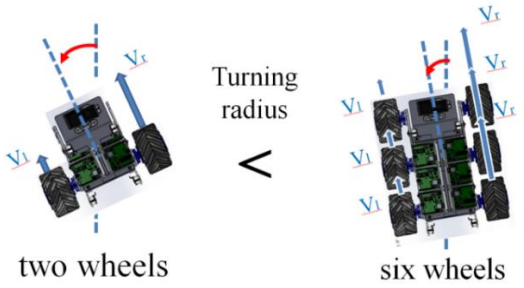

Figure 10: Turning radus of two wheels and six wheels.

Basic characteristics of the turning radius are described in the six-wheeled vehicle model simulator described in one report [24] and the turning method for multi-wheeled vehicles described in another report of the literature [25]. According to those earlier studies [24] and [25], given a greater number of wheels of the driving unit and sufficiently large ground area, then resistance during turning is greater, as is the turning radius (Fig. 10). For two wheels, the turning radius is the distance between the centers of the left and right tire widths when only one wheel is turned. The calculated value is 110 mm if one calculates the turning radius based on the FSR size. In reality, the turning radius will be larger because the ground resistance of FSR with six wheels is greater than that of two wheels.

To measure the turning radius repeatedly for the experiment, we used a board floor, which ensures more level ground than on soil, such as on a farm. We sent a left turn command from our smartphone application and drove until the FSR turned 90 degrees. The speed settings for each wheel were 100 min^{-1}, which is the minimum speed at which the prototype can drive. The speed at which it stops was set to 0 min^{-1}. However, the wheels are not braked. Therefore, the wheels will turn if an external force is applied. Table 2 shows the turning radius resulting from the difference in the way the left and right wheels turn. The measured values in Table 2 are average values of 10 measurements in each case. The case of the spin turn caused by driving with all left wheels backward and all right wheels forward was excluded because it rotates around the chassis.

From the cases shown in Table 2, one can select a useful movement method for turning. The method in case 1 operates only one wheel. The turning radius value of case 1 was 2,134.4 mm. The radius required for turning among fruit trees varies. General fruit tree spacing is 4,000 mm [26].

Table 2: Turning radii of different left and right wheel turn modes (fixed rotation speed of the left wheel)

	Pattern	Average turning radius [mm]
case 1	Right Wheels: forward Left Wheels Front, Middle, Rear: stop	2,134.4
case 2	Right Wheels: forward Left Wheels Front: stop, Middle, Rear: back	2.6 Near spin turn
case 3	Right Wheels: forward Left Wheels Front, Rear: back Middle: stop	3.2 Near spin turn
case 4	Right Wheels: forward Left Wheels Front, Middle: back Rear: stop	2.1 Near spin turn
case 5	Right Wheels: forward Left Wheels Front, Rear: stop Middle: back	145.3
case 6	Right Wheels: forward Left Wheels Front, Middle: stop Rear: back	457.7
case 7	Right Wheels: forward Left Wheels Front: back Middle, Rear: stop	121.0

Case 1 was found to be sufficiently operational as an orchard turning radius. However, spacing between fruit trees in a small orchard is 1,000 mm [22], making it difficult to operate with the turning radius of case 1 operation.

The salient point, as shown for cases 2–7, is that we conceived a method to reduce the turning radius: we drive the left wheels, actually, three wheels, backward when turning left. Cases 2–4 had a turning radius close to that of a super new land turn. The common feature was that two wheels on each side were driven backward. Therefore, after we chose the rotation pattern to be used for turning from cases 5–7, we measured the angle change during rotation in case 5–7 patterns using the gyro-sensor attached to the FSR. Figure 11 portrays a graph of the change in rotation angle for cases 5–7. The horizontal axis is the time spent for a 90-degree turn. The vertical axis is the angle measured by the gyro sensor. In case 6, the return of rotation is large. It can be confirmed that it shakes during rotation. We assume that this large rotation occurs because the battery is located behind the FSR. Therefore, the center of gravity is behind it. We expect the slippage to be large and expect that shaking occurred. If the oscillation is large, then stable observations such as those by image recording by the camera cannot be expected. Therefore, it is necessary to select case 5 and case 7 for observations. For this study, case 7 was used to ascertain whether the turning radius increases because of the speed difference between the left and right wheels. Table 3 presents results obtained from increasing the rotation speed of the right wheel in the rotation pattern of case 7. Increasing the rotation speed of the left wheel caused a larger

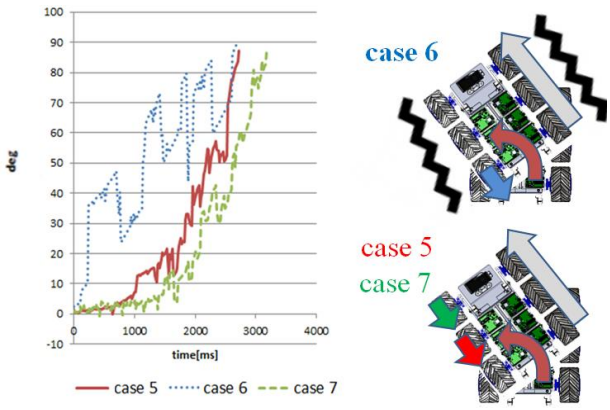

Figure 11: Change in rotation angle during FSR rotation.

Table 3: Turning radius associated with different turning of the left and right wheels (fixed right wheel rotation speed)

	Pattern	Average turning radius [mm]
case 7-1	Right Wheels: forward (100 [min^{-1}]) Left Wheels Front: back (110 [min^{-1}]) Middle, Rear: stop	152.6
case 7-2	Right Wheels: forward (100 [min^{-1}]) Left Wheels Front: back (120 [min^{-1}]) Middle, Rear: stop	176.4

turning radius. Through these experiments, we were able to find a way to change the FSR turning radius. Subsequently, turning was performed on soft soil using case 1 in Table 2. The turning radius was 1,962.9 mm (91.9% of the turning radius of the floor). Wheel slippage was observed. In case 7, slippage was then observed on the left front wheel driving backward. The measured value was 100.2 mm (82% of the turning radius of the floor). To counteract slippage, the ground contact area of the wheels must be reduced, as in ordinary vehicles. For that reason, the wheel tire width must be narrowed.

4.2 Drive on Uneven Terrain

It is necessary to evaluate whether the FSR frame will allow the vehicle to be stable on uneven terrain while driving. Figure 12 shows a test course with a 30 mm step used to verify that the FSR can maintain the same level of wheel contact as in the CAD simulation. The step is set at 30 mm because the FSR is calculable to overcome heights up to half of the tire diameter because of the link structure design. The FSR ran at the same speed as the mobility experiment. On the course, the convex part is blue. The concave part is red. As a result of visual checking of the ground contact, FSR confirmed that the six wheels were installed on bumpy ground (Fig. 13).

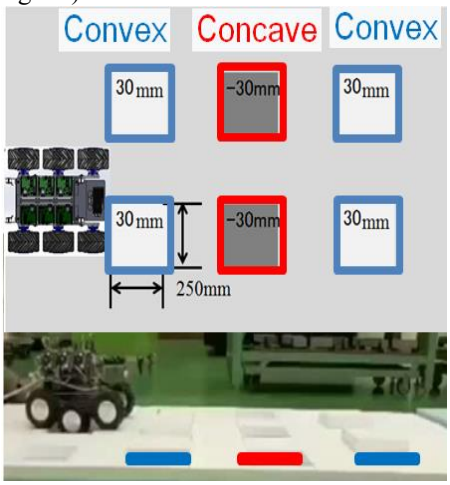

Figure 12: Ground contact performance on a test course with 30 mm bumps.

Figure 13: Driving of FSR with high grounding capacity.

Figure 14: Driving the FSR on the uneven farm.

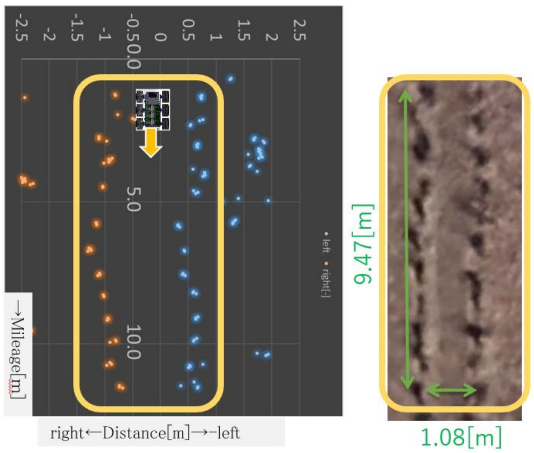

Figure 15: Measurement of tree position (left, measurement result; right, actual orchard).

The FSR was driven in a mulberry field to evaluate driving on uneven terrain (Fig. 14). The FSR used 2D-LiDAR to measure the distance of fruit trees and avoid fruit trees while driving. To detect the fruit tree position, the distance of fruit trees on either side of the FSR was measured. Figure 15 shows the measurement results. The FSR meandered as it took measurements, which distorted the measurement results. Nonetheless, results demonstrated that actual tree positions in the field were identifiable from the tree data.

We confirmed that the FSR obtained good driving performance on a field with numerous small obstacles such as pebbles and branches.

4.3 Observation of Leaf Undersides

Facilitated by the advancement of artificial intelligence (AI, especially machine learning) technology, many research results have been reported [27]. To build a practical system, pre-processing is necessary to judge the recorded crop images properly before analysis by machine learning. Images are taken over a wide area to obtain numerous images from fixed-point observations.

The training data used in the discriminator are diagnostic images from a single leaf, as represented by Plant Village, a well-known dataset on leaf diseases. More is learned from wide area photographs, and lower accuracy of identification is obtained for different farms. Therefore, pre-processing is necessary to extract a single leaf from a wide area photo.

In addition, regularization, such as data augmentation and dropout, is effective as a method to suppress overlearning. Background removal is also effective before regularization.

In FSR observations, one can observe the underside of leaves, whereas the sky occupies most of the background by close observation while moving the crop. By reducing the number of useless background images, the background removal process can be shortened. Furthermore, by correlating the RTK-GNSS coordinates with the acquired images, one can photograph only those areas where disease or insect damage is detected.

In this experiment, the images observed by looking up are sent to an AI-based image discrimination application for

Table 4: Observation results for the mulberry farm

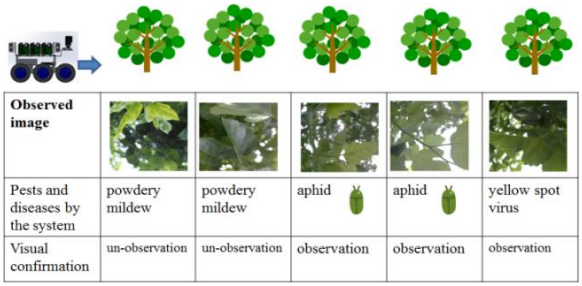

Observed image					
Pests and diseases by the system	powdery mildew	powdery mildew	aphid	aphid	yellow spot virus
Visual confirmation	un-observation	un-observation	observation	observation	observation

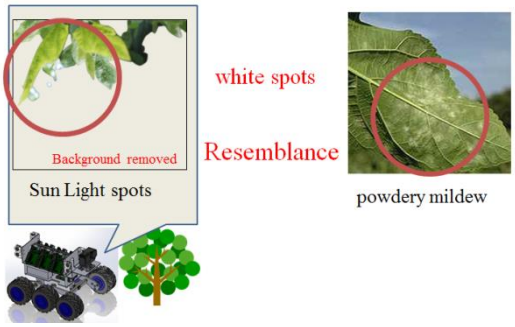

Figure 16: No powdery mildew symptoms.

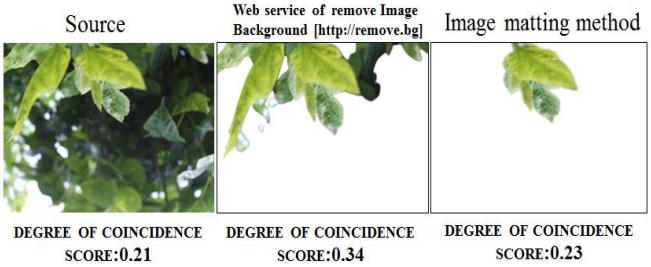

Figure 17: Match score under background removal.

discrimination. If one can make no determination, then the background can be deleted to verify whether a correct decision can be made.

Using sensors embedded in the FSR, we experimented to observe whether pests and diseases are visible from the observation results. Table 4 presents observation results obtained for the mulberry farm. For the diagnosis of diseases and insects, we used PlantMD [28], an AI-based smartphone application that estimates diseases and pests from images. Mulberry trees on the farm were photographed from above. Rows of trees without disease were selected. We drove the FSR along the side of the crops and looked up to observe them. After sending the acquired images to PlantMD for diagnosis of pests and diseases, we checked the location at which we obtained powdery mildew detection results. Nevertheless, no powdery mildew symptoms were found (Fig. 16). Powdery mildew causes white spots on the leaf surface. When images were checked, we were able to observe that the leaves had spots through which light shone because of backlighting. We presumed that these points were misdiagnosed as powdery mildew.

Therefore, background removal was achieved using a web service (remove. bg), with foreground extraction using an

Alpha Matting technique. PlantMD, which can measure disease concordance (Fig. 17), was used to measure the score for powdery mildew. Figure 14 presents the results. All of the diseases were diagnosed as powdery mildew. The effect of the background was determined as minimal. During operation, it is necessary to find a threshold of the detected scores and to consider new powdery mildew detection methods.

We then obtained aphid detection results from two locations. We confirmed the presence of aphids by checking the observed sites directly. Additionally, we observed a yellowing virus disease from one location. Direct confirmation of the area in which the virus was observed revealed a yellow discoloration. However, viral diseases are difficult to assess accurately because they require specialized analysis. Insect damage, however, is easy to detect even by people without specialized knowledge, allowing for rapid eradication of pests.

In addition, the duration of observation within the orchard was measured. Figure 18 shows the mulberry farm size and the number of rows of trees used for observation. FSR drove between the rows of trees from the bottom of the first row to the top of the seventh row in the mulberry field shown in Fig. 18, recording temperature and humidity along with images of leaf undersides. The measurement duration was 2 min and 10 s. The observed data are presented in Figs. 19 and 20. The heat map facilitates easy identification of observation locations.

5 CONCLUSIONS

This study revealed that FSR has the potential to provide crop-specific observation information necessary for decision-making in precision agriculture while driving between crops. The FSR has a simple configuration with a frame that has an in-wheel motor and a linkage mechanism. Nonetheless, the FSR can run on uneven terrain with branches and soil irregularities. We discovered the possibility of detecting environmental values such as leaf underside images, temperature, and humidity while driving between rows of crops by the FSR.

Additional accuracy is necessary for driving and observation locations. The FSR can produce observations of crop variation and can support farmers' decision-making by showing data for locations within their farms.

Future work includes developing a method for pest and disease prediction and detection based on observed images of pests and diseases, time, temperature, humidity, and other observed values obtained using detection technology. Furthermore, to enable autonomous operation, a patrol function based on longitude and latitude information from Camera, LiDAR, and RTK-GNSS is required. It must meet technical standards for automatic operation set by the Ministry of Agriculture, Forestry, and Fisheries [29].

ACKNOWLEDGMENTS

We would like to express appreciation to Professor Kaori Fujinami of the Tokyo University of Agriculture and Technology for expert advice on our research.

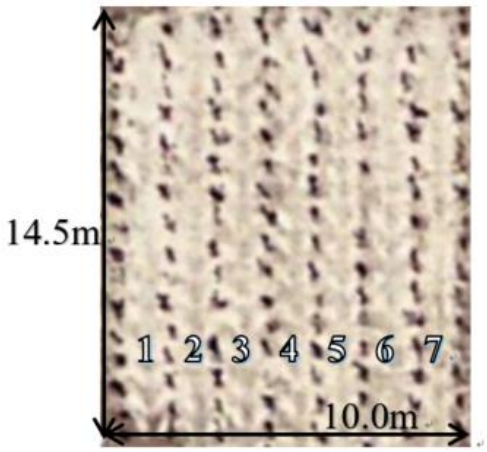

Figure 18: Dimensions and number of trees on the orchard.

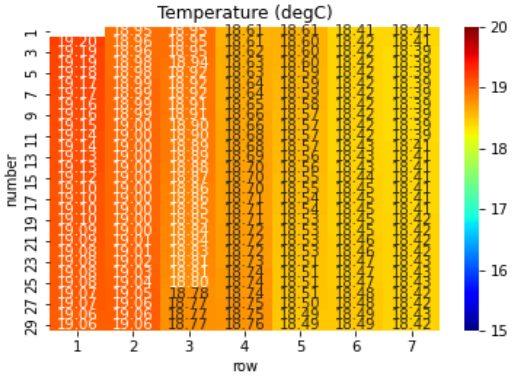

Figure 19: Heat map of orchard temperature.

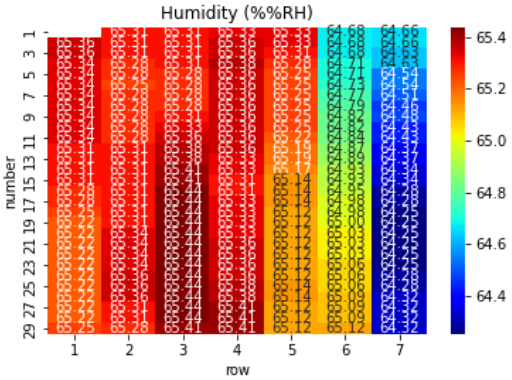

Figure 20: Heat map of orchard humidity.

REFERENCES

[1] Statistics of Agriculture, Forestry and Fisheries, MAFF, pp. 11-7 (2020).
[2] E. Shibusawa, “Precision Agriculture”, Asakura Publishing Co., Ltd.(2006).
[3] J. Champ, A. Mora-Fallas, H. Goëau, E. Mata-Montero, P. Bonnet, “Instance segmentation for the fine detection of crop and weed plants by precision agricultural ro-

bots," Applications in Plant Sciences, Vol. 8, No. 7 (2020).
[4] O. Spykman, A. Gabriel, M. Ptacek, M. Gandorfera, Farmers' perspectives on field crop robots – Evidence from Bavaria, Germany, < https://www.sciencedirect.com/science/article/pii/S0168169921001939 > ,[referred May 2021].
[5] "midori cloud (in Japanese)", < https://info.midori-cloud.net/vision/>,[referred May 2021].
[6]] H. Iyatomi, "Trends and Challenges of Automatic Diagnosis Techniques for Plant Diseases," Japanese Neural Network Society Journal, Vol. 26, No. 4, pp. 123–144 (2019).
[7] D. Mhlanga, Artificial Intelligence (AI) and Poverty Reduction in the Fourth Industrial Revolution (4IR). Preprints 2020, 2020090362 (doi: 10.20 944/ preprints-202009.0362.v1). (2020).
[8] "SCIBAI (in Japanese)", < https://www.mirai-scien.com >, [referred May.2021].
[9], N.S. Naik, V.V. Shete, and S.R. Danve, "Precision agriculture robot for seeding function," 2016 International Conference on Inventive Computation technologies (ICICT). Vol. 2. IEEE(2016).
[10] R. Sugiura, "Remote sensing for large-scale field information using drone imagery," Research Center for Agricultural Information Technology, pp. 184–187 (2020).
[11] S. Yamamoto, "Fundamental Study on the Collection of Big Data for the Agricultural Community Using Machine Vision: Exploring a Potential Technology to Complement Drone Information for Monitoring Plants," Akita Prefectural University Web Journal B, pp. 85–90 (2018).
[12] Ministry of Agriculture, Forestry and Fisheries, pest control,<https://www.maff.go.jp/j/seisan/kankyo/hozen_type/h_sehi_kizyun/attach/pdf/aki3-15.pdf>, [referred Oct .2021].
[13] Changes and Issues Concerning Plant Protection, <https://www.maff.go.jp/j/syouan/syokubo/keneki/attach/pdf/arikata-14.pdf >, [referred Mar.2021].
[14] K. Oshima, "Plant potyvirus evolution the survey of the genetic structure of populations," Virus, Vol. 2, pp. 151–160 (2012).
[15] M. Arun et al., "Smart Agriculture Robot," International Journal of Pure and Applied Mathematics, Vol. 119, No. 15, pp. 1901–1906 (2018).
[16] "avo", <https://www.ecorobotix.com/en/avo-autonomous-robot-weeder/>, [referred Mar.2021].
[17] "Weed Whacker", < https://www.odd.bot/>, [referred Feb.2021].
[18] "DICK", <https://www.smallrobotcompany.com/>, [referred Oct.2021].
[19] A. Schafer et al., "Robot Mobility Concepts for Extra-terrestrial Surface Exploration," IEEE, Aerospace Conference, pp. 1–12 (2008).
[20] Y. Hirota, Electric vehicle engineering (in Japanese), Morikita Publishing Co., Ltd. pp. 60–66 (2017).
[21] T. Hiroki et al., "Diagnosis of multiple cucumber infections with convolutional neural networks", IEEE Proc. AIPR, pp. 104 (2018).
[22] The National Agriculture and Food Research Organization, "Small Fruit Tree Manual (in Japanese)," (2018).
[23] Ministry of Health, Labour and Welfare, "Physical activity standards for health in 2013," pp. 51 (2013).
[24] M.H. Prio, F. Rios, "Kinematic Modeling of a Six Wheeled Differential Drive Intelligent Robot and Potential Field Method to Attain Obstacle Avoidance Capability," 2019 Southeast Con., pp. 1–4 (2019).
[25] N. Ito, N. Iguchi, "Steerability Control of Multi-Powered Wheel Vehicle," JSAM Journal, Vol. 50, No. 1, pp. 11–18 (1988).
[26] "How to plant fruit tree seedlings (in Japanese)",< https://minorasu.basf.co.jp/80083>, [referred Mar.2021].
[27] H. Iyatomi, "Trends and Challenges of Automatic Diagnosis Techniques for Plant Diseases," Neurology and Clinical Neuroscience, Vol. 26, No. 4, pp. 123–134, (2019).
[28] "PlantMD", <http://plant-md.org/>, [referred Oct 2021].
[29] The National Agriculture and Food Research Organization, "Small Fruit Tree Manual (in Japanese)", (2018).

(Received: October 30, 2021)
(Accepted: August 2, 2022)

Kenji Terada earned a B.E. degree from Polytechnic University, Tokyo and graduated from the course of Electrical Engineering and Computer Science, Graduate School of Engineering Polytechnic University. He is currently an Associate Professor of Polytechnic University, Tokyo. He received a Master's degree in Industrial Engineering from NIAD-UE Tokyo in 2002.

Masaki Endo earned a B.E. degree from Polytechnic University, Tokyo and graduated from the course of Electrical Engineering and Computer Science, Graduate School of Engineering Polytechnic University. He received an M.E. degree from NIAD-UE, Tokyo. He earned a Ph.D. Degree in Engineering from Tokyo Metropolitan University in 2016. He is currently an Associate Professor of Polytechnic University, Tokyo. His research interests include web services and web mining. He is also a member of DBSJ, NPO STI, IPSJ, and IEICE.

Takuo Kikuchi received a Ph.D. degree in Engineering from Kyushu Institute of Technology. He is currently a professor of the Dept. of Electrical and Computer Engineering at Polytechnic University. His research interests include "Information network cabling" and "Skill analysis and evaluations". He is a member of JSEE, IEICE, and JSET Japan.

Shigeyoshi Ohno earned M.Sci. and Dr. Sci. degrees from Kanazawa University and a Dr. Eng. degree from Tokyo Metropolitan University. He is currently a full Professor of Polytechnic University, Tokyo. His research interests include big data and web mining. He is a member of DBSJ, IPSJ, IEICE and JPS.